

A point cloud-based welding trajectory planning method for plane welds

Yuankai Zhang

Yong Jiang

Xincheng Tian (✉ txch@sdu.edu.cn)

Shandong University, China

Xiaolong Xu

Yusen Geng

Min Lai

Research Article

Keywords: 3D vision, Weld seam extraction, Point cloud feature extraction, Without teaching and programming, Welding path planning

Posted Date: August 8th, 2022

DOI: <https://doi.org/10.21203/rs.3.rs-1908430/v1>

License: © ⓘ This work is licensed under a Creative Commons Attribution 4.0 International License.

[Read Full License](#)

6
7
8
9
10
11
12 A point cloud-based welding trajectory planning method for
13 plane welds
14
15
16

17 Zhang Yuankai^{1,2}, Jiang Yong^{1,2}, Tian Xincheng^{1,2*}, Xu Xiaolong^{1,2*}, Geng Yusen^{1,2}
18 and Lai Min^{1,2}
19

20 ¹Center for Robotics, School of Control Science and Engineering, Shandong University,
21 Jingshi Road, Jinan, 250061, Shandong, China.

22 ²Engineering Research Center of Intelligent Unmanned System, Ministry of Education,
23 Jingshi Road, Jinan, 250061, Shandong, China.
24
25

26
27 *Corresponding author(s). E-mail(s): txch@sdu.edu.cn; xxl@sdu.edu.cn;
28
29

30
31 **Abstract**

32 Plane welds are a common type of weld in industrial sites. When the welding robot welds multiple
33 types of plane welds at the same time, the traditional teaching and programming modes become
34 relatively complicated. Therefore, in order to solve the problem of automatic robot welding of various
35 types of plane welds, taking plane V-type butt, plane I-type butt, and plane lap welds as examples,
36 this paper proposes a plane weld extraction method based on 3D vision. Firstly, in order to realize
37 the line and plane segmentation of the workpiece point cloud, we establish the concept of plane point
38 cloud density. Secondly, to segment workpiece edge lines, an iterative segmentation algorithm based
39 on RANSAC is proposed. Then, based on the geometric features of the workpiece, a method for
40 extracting weld feature points based on centroid positioning is proposed. Finally, the least squares
41 method is used to fit the feature points of the welding seam to complete the welding trajectory
42 planning. The experimental results show that the method can well solve the problem of automatic
43 planning welding trajectory of plane V-type butt, plane I-type butt, and plane lap welds, to realize that
44 the welding robot can simultaneously weld various plane welds without teaching and programming.

45 **Keywords:** 3D vision, Weld seam extraction, Point cloud feature extraction, Without teaching and
46 programming, Welding path planning
47
48
49

50 **1 Introduction**

51
52 Traditional manual welding has shortcomings such
53 as high technical requirements for personnel, poor
54 working environment, poor consistency of weld-
55 ing quality, and low welding efficiency. In order
56 to overcome the above shortcomings, welding
57 robots have begun to be widely used in industrial
58 scenarios[1].At present, the welding robot relies
59 on robot programming to realize automatic weld-
60 ing. The traditional robot programming methods

include manual teaching programming and offline
programming (OLP)[2, 3].However, the manual
teaching programming workload is large, and the
clamping accuracy of the workpiece is relatively
high. The offline programming highly depends on
the CAD model of the workpiece, and the pro-
gramming is complicated. In recent years, some
researchers have gradually used structured light
vision sensors to guide robotic welding, to achieve

intelligent welding with less programming and free programming.

A structured light vision sensor generally consists of a laser transmitter and a camera, whose measurement principle is optical triangulation[4–6].According to the different types of emitted lasers, structured light vision sensors can be roughly divided into line structured light vision sensors and area array structured light vision sensors.

The welding seam feature extraction methods based on the line structured light vision sensor process the RGB-D information. Xu et al. extracted the feature points of the weld by improving the canny algorithm, and then matched the depth information to obtain the three-dimensional information of the feature points of the weld, and finally realized the real-time tracking of the weld of argon tungsten arc welding (GTAW)[7].The welding seam information obtained using a single line laser is limited, and the feature extraction algorithm has limitations. Therefore, some researchers achieve a better weld extraction effect by changing the amount and type of structured light[8, 9].Such as, Shao et al. changed the number of laser stripes and the wavelength of the laser. They combined the measurement information obtained by different wavelengths of lasers to calculate and designed an extraction method of I-type narrow welds[10]. Gao et al. studied the interference problems such as arc light in welding. They optimized the dark channel prior anti-jamming processing algorithm based on contour and OTSU threshold, which can effectively remove metal vapor and plasma sputtering during welding[11].The research on weld feature extraction methods based on the line structured light vision sensor is relatively mature. However, line structured light vision sensors can only be used for welding seam tracking due to the limitation of their own information acquisition, and rough teaching of the welding path is still required before welding. Therefore, those methods have little effect on the programming simplification of the robotic welding process.

Area array structured light vision sensors are known as area array structured light cameras or 3D cameras. Compared with the linear structured light vision sensor, the spatial information obtained by the area array structured light vision sensor is more abundant. Therefore, using area

array structured light to guide robotic welding can further simplify the programming effort.

There are mainly two types of welding seam feature extraction methods based on area array structured light camera. One is to process the obtained RGB-D information[12–14].The essence of such methods is to process two-dimensional images. It is more sensitive to light, so this type of method is generally not used in industrial sites. The other is to process point cloud information. Then, point cloud-based weld feature extraction methods can be divided into two categories. The first class of methods is based on the local features of point clouds[15, 16].For example, Gao et al. studied the spatial curve weld and extracted the spatial weld using the point cloud’s normal feature [17].The second class of methods is based on the global geometric features of point clouds [18, 19].For example, Yang et al. proposed a weld extraction method based on the point-to-plane distance for plane butt V-type welds and realized the extraction of plane V-type welds[20].

Plane welds generally refer to plane butt welds and plane lap welds, which are common types of weld joints spliced between sheets and are extremely common in the industry. However, there are the following difficulties in using the existing point cloud-based methods to extract plane welds:

1. When using the method based on the local features of point clouds to extract the weld seam, the difficulty is that the local features of the neighboring points tend to be consistent, which makes it difficult to distinguish the feature points and non-feature points.
2. When using the method based on the global geometric features of point clouds to extract the weld, the difficulty lies in the poor adaptability of the method, and different judgment rules need to be set for each specification of the weld joint.

In order to overcome the above difficulties, this paper proposes a feature extraction method for plane welds based on plane point cloud density. The main contributions of this paper are as follows:

1. This paper realizes the efficient and accurate segmentation of the plane and line features of the point cloud by combining the local features

- of the point cloud with the imaging principle of the area array structured light camera.
- This paper fully uses the common geometric features of plane welds and is suitable for weld extraction of plane V-type butt welds, plane I-type butt welds, and plane lap welds.
 - A comparative experiment is designed, and the accuracy and feasibility of the proposed method are verified by error analysis.

This article is organized as follows: Section 2 introduces the composition and framework of the experimental system in detail. Section 3 proposes a line and plane classification method of the plane weld workpiece model based on plane point cloud density. Section 4 presents a method for extracting weld seam features based on centroid positioning. Section 5 is the analysis of experiments and results to verify the feasibility, accuracy, and efficiency of the method in this paper. Section 6 concludes the work of this paper.

2 System configuration and framework

2.1 System platform

As shown in Fig. 1, the composition framework of the robot welding experimental platform built in this paper mainly includes the welding execution system and the 3D vision system. The welding execution system is mainly composed of a robotic arm and welding equipment. It realizes the photographing action and welding action. The 3D vision system is mainly composed of an area array structured light camera and an industrial computer. Its main functions include the acquisition of 3D point cloud information, the extraction of weld features, and the planning of welding trajectories. The two systems are connected by TCP/IP communication.

In order to photograph the weld area of the workpiece more flexibly, the area array structured light camera and the robot are combined in the Eye-in-Hand manner. The parameters of the area array structured light camera selected in this experiment are shown in Table 1.

2.2 Workpiece model

In this paper, the plane V-type butt joint, the plane I-type butt joint, and the plane lap joint

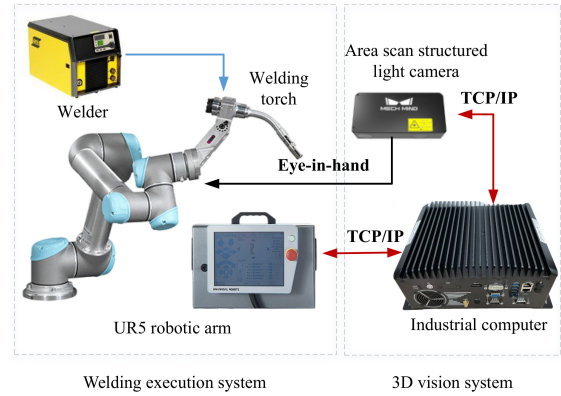


Fig. 1 The composition of the experimental system

Table 1 Parameters of the area array structured light camera in this experiment

Parameter	Value
Recommended working distance range(mm)	500-1000
Near-end field of view (mm)	350×220 @ 0.5m
Far field of view (mm)	700×440 @ 1m
Resolution	1920×1200
The number of pixels	2.3MP
Nominal accuracy	0.1mm
Typical acquisition time	0.5s-0.8s
The length of the baseline	150mm
Overall dimensions	270×72×130mm
Weight(kg)	2.2

among the plane weld types are selected for research. As shown in Fig. 2, this study built three workpiece models of welded joints in the laboratory environment. Fig. 2(a) is the workpiece model of plane V-type butt joint, Fig. 2(b) is the workpiece model of plane I-type butt joint, and Fig. 2(c) is the workpiece model of plane lap joint.

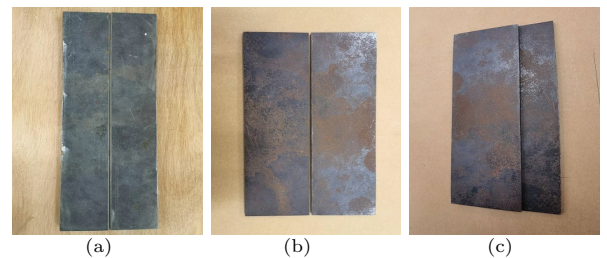


Fig. 2 Plane weld workpiece models

2.3 System framework

In this experiment, the 3D camera shoots the workpiece to form a point cloud and transmits the point cloud data to the industrial computer through TCP/IP. The point cloud is processed on the industrial computer. First, in order to simplify the extraction of weld features, the initial point cloud is preprocessed to obtain the three-dimensional information of the workpiece. Then, according to the workpiece's three-dimensional information, the weld's feature is extracted, and the welding trajectory is planned. Finally, the industrial computer transmits the welding trajectory data to the robot controller through TCP/IP, and the robot executes the welding trajectory motion. The system framework flowchart is shown in Fig. 3.

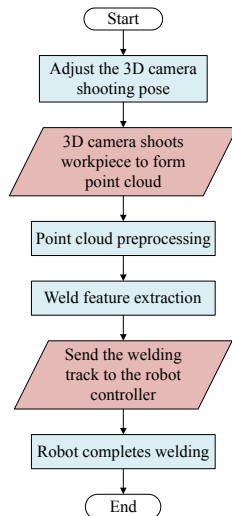


Fig. 3 System framework flowchart

3 Point cloud preprocessing

The geometric features of the plane weld workpiece are composed of simple lines and planes. To extract the weld feature points, it is necessary to analyze the lines and planes information of the plane weld workpiece. In order to extract the plane points and line points of the point cloud of the plane weld workpiece, this paper proposes the concept of plane point cloud density. On this basis, the plane point criterion and the plane edge point criterion are set.

3.1 Plane point cloud density

Fig. 4 shows the measurement principle of the area array structured light camera. The area array structured light projected by the laser projector is modulated by the object surface, collected by the camera, and transmitted to the computer. Then, by analyzing and calculating the original data using the principle of pinhole imaging and triangulation[21], we obtain the point cloud data of the measured surface in the camera coordinate system with the camera optical center as the origin.

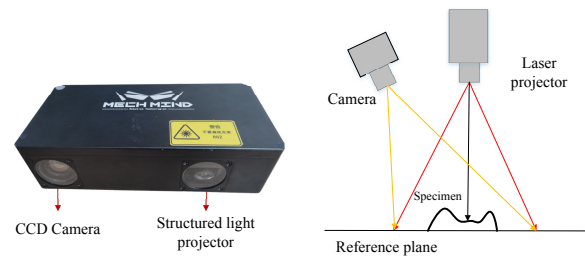


Fig. 4 Measurement principle of area array structured light camera

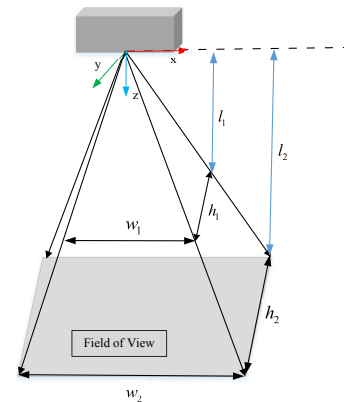


Fig. 5 Schematic diagram of the 3D camera field of view

As shown in Fig. 5, the field of view of the area array structured light camera refers to the plane parallel to the xoy plane of the camera coordinate system that is covered by the structured light within the working distance of the camera. Due to the property of light traveling in a straight line, the width and height of the field of view are proportional to the distance from the field of view to

the camera coordinate xoy plane.

$$\frac{l_1}{l_2} = \frac{w_1}{w_2} = \frac{h_1}{h_2} \quad (1)$$

Therefore, we set the width and height of the field of view as W and H , respectively. The distance from the field of view to the xoy plane of the camera coordinate system is denoted by L . We can get Eq. 2. Since the field of view is parallel to the xoy plane of the camera coordinate system, L can be measured using the z coordinate in the camera coordinate system.

$$W = \frac{w_1}{l_1}L, \quad H = \frac{h_1}{l_1}L \quad (2)$$

The area of the camera's field of view S can be obtained by:

$$S = W \times H = \frac{w_1 h_1}{l_1^2} L^2 \quad (3)$$

Let F be the resolution of the area array structured light camera. Then we can calculate the plane point cloud density D as:

$$D = \frac{F}{S} = \frac{F l_1^2}{w_1 h_1 L^2} \quad (4)$$

For plane weld workpieces, when the 3D camera shoots with the z -axis of the camera coordinate system perpendicular to the workpiece plane, the workpiece plane coincides with the field of view. The obtained plane point density on the workpiece point cloud satisfies Eq. 4. Therefore, the plane point cloud density can be used as a theoretical basis for dividing the line and plane of the workpiece.

According to Table 1, the resolution of the area array structured light camera used in this paper is 1920×1200 . We set $l_1 = 1000mm$, $w_1 = 700mm$, $h_1 = 440mm$, and substitute them into Eq. 4:

$$D = \frac{1920 \times 1200}{S} = \frac{2.304 \times 10^9}{308L^2} \quad (5)$$

3.2 Plane point cloud extraction

3.2.1 Theoretical number of neighborhood points

In this experiment, we define a standard 3D camera pose for shooting in which the z -axis of the camera coordinate system is perpendicular to the plane weld workpiece. For the workpiece point cloud captured in this posture, the point cloud density of the plane point can be calculated by Eq. 5. At this point, we delineate a nearby area of radius R for any plane point. The product of its density and the area of the nearby area is the theoretical number of neighborhood points N :

$$N = \pi \times R^2 \times D = \frac{2.304\pi R^2 \times 10^9}{308L^2} \quad (6)$$

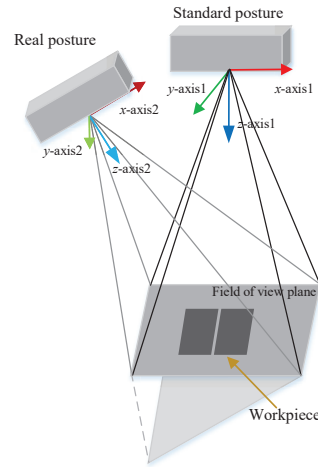


Fig. 6 Schematic diagram of camera shooting pose

However, in the actual operation process, it is tough to control the robot's end to achieve the standard posture for shooting. As shown in Fig. 6, under the non-standard shooting posture, the obtained plane point cloud has a certain inclination angle with the camera's field of view plane, which will cause the plane point cloud density to be uneven. At this time, using Eq. 6 to obtain the number of theoretical neighborhood points for plane points will lead to errors. Therefore, we need to analyze this error.

As shown in Fig. 7, in the plane point cloud with an included angle of θ to the field of view

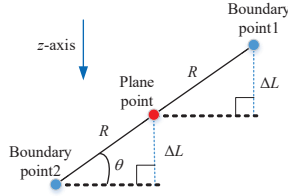


Fig. 7 Schematic diagram of camera shooting pose

plane, we select a point to find a neighborhood with a radius R and select two edge points in the direction of the plane's inclination. In the neighborhood area, the difference between the two edge points and the center point is the largest on the z -axis:

$$\Delta L = R \sin \theta \quad (7)$$

By analyzing the function characteristics of Eq. 4, we know that among all the neighboring points, the difference between the plane point cloud density of the Boundary point1 and the center point is the largest, so there are:

$$\begin{aligned} \Delta D &= \frac{2.304 \times 10^9}{308(L - \Delta L)^2} - \frac{2.304 \times 10^9}{308L^2} \\ &= \frac{2.304 \times 10^9}{308} \times \frac{2L\Delta L - \Delta L^2}{L^2(L - \Delta L)^2} \end{aligned} \quad (8)$$

From Eq. 8, we can estimate the maximum error in finding the theoretical number of neighborhood points in the neighborhood as:

$$E_1 = \pi R^2 \Delta D \quad (9)$$

The recommended working distance range of the camera in this experiment is $500mm - 1000mm$. At this time, Eq. 9 is a decreasing function. When $L = 500mm$, E_1 takes the maximum value:

$$E_1|_{L=500} = \frac{2.304 \times 10^9}{308} \times \frac{1000\Delta L - \Delta L^2}{500^2(500 - \Delta L)^2} \pi R^2 \quad (10)$$

After a lot of experiments, when the camera is shooting, its posture can generally keep the angle between the z -axis and the normal of the work-piece plane less than 30 degrees, namely $\theta < 30^\circ$. Moreover, the neighbor radius R in this experiment is $1mm$. Substituting $R = 1mm$ and $\theta = 30^\circ$ into Eq. 10, the maximum error of the theoretical number of neighborhood points brought

by the shooting posture can be reduced to 0.06. Therefore, this error can be ignored.

3.2.2 The plane point criterion

There is a certain measurement error in the point cloud obtained by the 3D camera, which will result in the calculation error of the area of the neighbor area. This is another error source in the theoretical number of neighborhood points. The utilized 3D camera has a nominal error of $0.1mm$ within a working range of $1000mm$. Let e be the measurement error of R , then $-0.1mm \leq e \leq 0.1mm$.

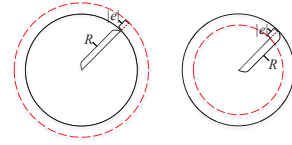


Fig. 8 Schematic diagram of the area error of the nearest neighbor circle

As shown in Fig. 8, the red circle is the measured neighbor area, and the black circle is the theoretical neighbor area. Therefore, the calculation formula of the maximum error of the theoretical number of neighborhood points brought by the area of the neighbors is:

$$E_2 = \pi [(R + |e|)^2 - R^2] D \quad (11)$$

Since $R = 1mm$, substituting $L = 500mm$ and $|e| = 0.1mm$ into Eq. 11, the maximum value of E_2 can be obtained as 19.74. Therefore, this error cannot be ignored. At this point, Eq. 6 is corrected to obtain:

$$N' = \pi(R + e)^2 D \quad (-0.1mm \leq e \leq 0.1mm) \quad (12)$$

From the monotonicity of the function, we can get:

$$\begin{aligned} N'_{min} &= \frac{2.304 \times 10^9 \pi (R - 0.1)^2}{308L^2}, \\ N'_{max} &= \frac{2.304 \times 10^9 \pi (R + 0.1)^2}{308L^2} \end{aligned} \quad (13)$$

For any point in the point cloud, the nearest neighbor search with radius R can get the actual number of neighbor points N_r . When the point is a plane point, N_r is greater than or equal to

the minimum value of N' . When the point is a non-plane point, the obtained N_r is less than the minimum value of N' because the laser light is blocked. According to the above theory, we can get the plane point criterion: for any point P in the point cloud, Eq. 14 is satisfied.

$$\begin{cases} P \text{ is a plane point,} & N_r \geq N'_{min} \\ P \text{ is a non-plane point,} & N_r < N'_{min} \end{cases} \quad (14)$$

In this experiment, we use the plane point criterion to extract the plane point cloud of the plane weld workpiece point cloud, and the result is shown in Fig. 9.

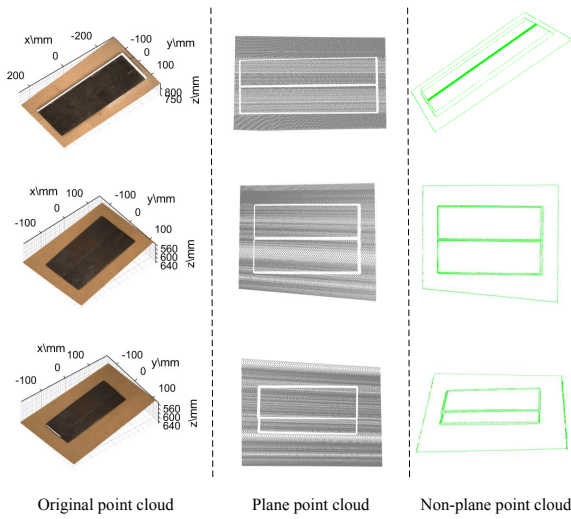


Fig. 9 Plane point cloud extraction

3.3 Remove the background from the workpiece

As seen from Fig. 9, the extracted plane point cloud contains the workpiece and background planes. We need to remove the background plane to facilitate further workpiece processing. We can see from the plane point cloud that the three planes are not connected. Therefore, in this experiment, the Euclidean clustering method is used to separate the three planes, then the three planes are identified, and the background plane is eliminated.

We set the threshold of Euclidean clustering to 2mm and divided the plane point cloud into three independent plane point clouds. As shown in Fig.

10, among the three planes, the xoy projection area of the background plane is the largest. This paper uses this feature to identify the background plane and delete it. However, the segmented point cloud is not a regular rectangle, so we construct a bounding box on the xoy plane according to the maximum and minimum values of the x and y coordinates of the point cloud. The point cloud with the largest projected area on the xoy plane has the largest bounding box on the xoy plane. Therefore, the point clouds of the workpiece plane are obtained by deleting the largest face of the xoy bounding box.

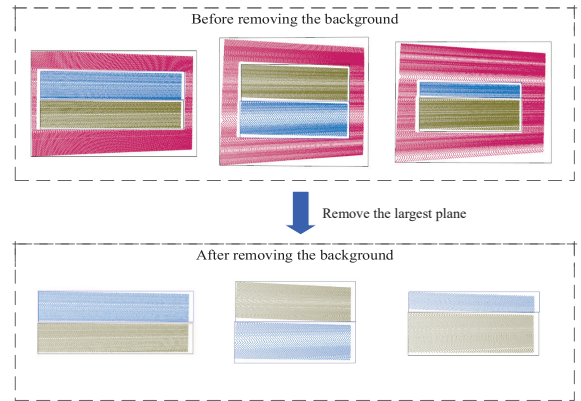


Fig. 10 Remove background plane

3.4 Extract workpiece edge lines

3.4.1 Extract the edge points of the workpiece

After the above point cloud processing, we have obtained the plane information of the plane weld workpiece. In this section, we extract the edge of the workpiece plane to get the line information of the workpiece.

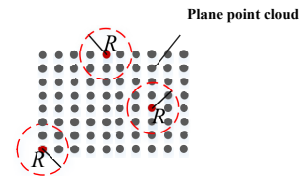


Fig. 11 Schematic diagram of the principle of plane edge point criterion

Each point's neighborhood of radius R is delineated on the plane point cloud. We can obtain each point's theoretical number of neighborhood points according to Eq. 6. However, as shown in Fig.11, edge points' actual number of neighborhood points is much smaller than their theoretical number of neighborhood points due to the limitation of the point cloud boundary. According to the above characteristics, we tend to find the nearest neighbor area for any point on the plane point cloud. When its actual number of neighborhood points N_r and its theoretical number of neighborhood points N satisfy $N_r < N \times \mu$ ($\mu < 1$), the point is regarded as an edge point. In order to accurately extract the edge, after experimental judgment, we finally determined the threshold $\mu = 0.5$. Therefore, the above theory is summarized into the plane edge point criterion of this experiment: for point P on the plane point cloud, Eq.15 is satisfied.

$$\begin{cases} P \text{ is a edge point,} & N_r \leq N \times 0.5 \\ P \text{ is a non-edge point,} & N_r > N \times 0.5 \end{cases} \quad (15)$$

According to the above criteria, the plane edge points are obtained from the workpiece plane point clouds. The results are shown in Fig.12, where the green and red dots represent the edge points of the two workpiece planes, respectively.

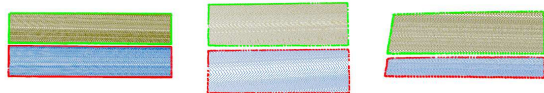


Fig. 12 Workpiece plane edge points extraction

3.4.2 Segment plane edge point cloud

Due to the disordered characteristics of the point cloud, the obtained workpiece plane edge point cloud is still indistinguishable edges. In this paper, the extraction of weld feature points requires the linear fitting of the point cloud of each edge. Therefore, we need to further segment the plane edge point cloud.

This paper proposes an iterative segmentation algorithm based on the Random Sample Consensus algorithm (RANSAC)[22] to segment all point

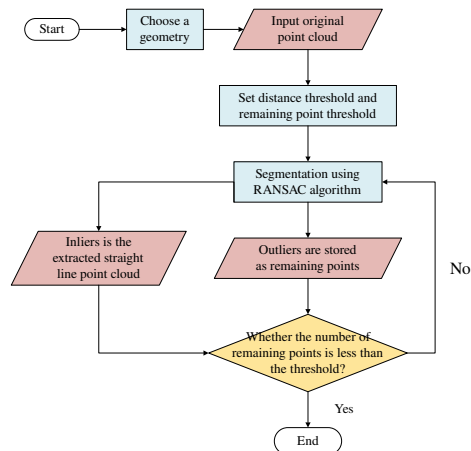


Fig. 13 An iterative segmentation algorithm based on RANSAC

cloud subsets with the same geometric model in a point cloud at one time. The algorithm has the following procedures. After selecting the geometric model, iteratively update the point cloud input to the RANSAC segmentation algorithm each time. Compare the number of the remaining points after segmentation with the set threshold of remaining points, and the point cloud less than the threshold will not be segmented. The specific steps are shown in Fig. 13. Finally, we set a threshold of $1mm$ and use this algorithm to segment the edge point cloud of the workpieces. The results are shown in Fig. 14, where different colors represent different plane workpiece edge lines.

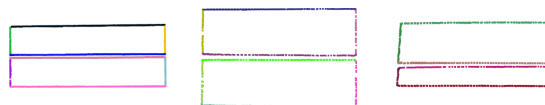


Fig. 14 Segmented edge point clouds

4 Weld extraction

4.1 Weld edge line extraction

By preprocessing the initial point cloud, we can get the workpiece's line and plane geometry information. On this basis, we extract the weld feature information. Aiming at plane weld workpieces, this paper proposes a method for extracting weld feature points based on centroid positioning. The

principle of this method is introduced by taking the plane I-type butt workpiece model as an example. As shown in Fig. 15, we first denote the extracted workpiece planes as Plane1 and Plane2. Then, the weld feature of the plane weld workpiece refers to the edges of the two planes on the side of the weld, denoted as Edge1 and Edge2, respectively. We find the centroids of Plane1 and Plane2, denoted as Centroid1 and Centroid2. It can be seen that, among all the edges, Centroid1 and Centroid2 are only distributed on both sides of Edge1 and Edge2. We refer to Edge1 and Edge2 collectively as the weld edge line. Due to the characteristics of affine transformation, when the workpiece plane point cloud is projected onto the xy plane, the above geometric features remain unchanged. Therefore, on the xy plane, the edge line of the weld can be extracted according to the position of the centroid of the two planes.

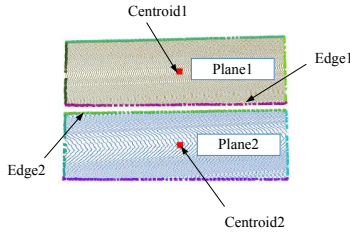


Fig. 15 Segmented edge point clouds

We assume that the projection equation of any one of the edge lines on the xy plane is $f_{edge}(x, y)$. The xy plane projection coordinates of Centroid1 and Centroid2 are denoted as $C1(x_{c1}, y_{c1})$ and $C2(x_{c2}, y_{c2})$, respectively. When Centroid1 and Centroid2 are distributed on both sides of an edge line, the following relationship exists.

$$f_{edge}(x_{c1}, y_{c1}) \times f_{edge}(x_{c2}, y_{c2}) < 0 \quad (16)$$

In section 3.4.2, we obtained the equations of these lines when using the RANSAC-based method to segment the plane edge point cloud. Therefore, we can extract the edge lines Edge1 and Edge2 of the weld using the above geometric principle. Finally, the extraction effect of the weld edge lines is shown in Fig. 16.

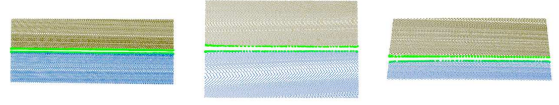


Fig. 16 Weld edge lines

4.2 Weld edge line fitting

Due to the limitations of the RANSAC algorithm, the equations of the extracted weld edge lines are not accurate enough and need to be re-fitted. Here, we use the least squares method for fitting.

The main idea of the least squares method is to solve the unknown parameters so that the sum of the squares of the difference between the theoretical value and the observed value is minimized. The observed value is multiple sets of samples, and the theoretical value is the value obtained by a hypothetical fitting function. For example, we have m samples $(x_i, y_i) (i = 1, 2, 3, \dots, m)$ with only one feature. The sample is fitted with a polynomial $h_t(x)$ of degree n .

$$h_t(x) = t_0 + t_1x + t_2x^2 + \dots + t_nx^n \quad (17)$$

In Eq. 17, $t(t_0, t_1, t_2, \dots, t_n)$ denotes the parameter to be solved. The residual sum of squares is:

$$C = \sum_{i=1}^m (h_t(x_i) - y_i)^2 \quad (18)$$

The least squares method considers that when C takes the minimum value, $t(t_0, t_1, t_2, \dots, t_n)$ is the optimal solution. The polynomial function at this time is the optimal fit of the sample. In this experiment, the matrix solution method of the least squares method is used to solve the parameters. Let the matrix expression of Eq. 17 be:

$$h_t(x) = X_v t \quad (19)$$

In Eq. 19, t is a vector composed of coefficients:

$$t = [t_0, t_1, t_2, \dots, t_n]^T \quad (20)$$

X_v is a Vandermonde matrix of dimension $m \times n$:

$$X_v = \begin{bmatrix} 1 & x_1 & x_1^2 & \dots & x_1^n \\ 1 & x_2 & x_2^2 & \dots & x_2^n \\ 1 & x_3 & x_3^2 & \dots & x_3^n \\ \vdots & \vdots & \vdots & \ddots & \vdots \\ 1 & x_m & x_m^2 & \dots & x_m^n \end{bmatrix} \quad (21)$$

The vector of sample observations is Y_o :

$$Y_o = [y_0, y_1, y_2, \dots, y_n] \quad (22)$$

So, the residual sum of squares can be written as:

$$C = (X_v t - Y_o)^T (X_v t - Y_o) \quad (23)$$

For the best fit, the derivative of Eq. 23 with respect to the t vector is equal to zero, as follows:

$$\frac{dC}{dt} = X_v^T X_v t - X_v^T Y_o = 0 \quad (24)$$

Finally, the solution formula of the parameter vector t can be obtained:

$$t = (X_v^T X_v)^{-1} X_v^T Y_o \quad (25)$$

The point cloud data is a three-dimensional data sample. We can complete the least squares polynomial fitting of the point cloud by selecting one-dimensional data as features and the other two-dimensional data as observations to form two sets of samples. The obtained two polynomials complete the description of the space curve. This experiment aims at the plane weld. For simplicity, we choose the dimension with a larger distribution range in x and y as the feature.

When x is selected as the feature, then y and z are respectively used as observations, and the samples are $(x_i, y_i), (x_i, z_i) (i = 1, 2, 3, \dots, m)$. When y is selected as the feature, then x and z are respectively used as observations, and the samples are $(y_i, x_i), (y_i, z_i) (i = 1, 2, 3, \dots, m)$.

For straight welds, we set the order n of the polynomial as 1. Finally, the fitting equations of the weld edge of the plane V-type butt workpiece model are obtained as Eq. 26 and Eq. 27. Eq. 28 and Eq. 29 show the fitting equations of the weld edge of the plane I-type butt workpiece model.

$$\begin{cases} y = -2.994 - 0.008626x \\ z = 771.948 - 0.127735x \end{cases} \quad (26)$$

$$\begin{cases} y = 6.986 - 0.008401x \\ z = 772.027 - 0.127357x \end{cases} \quad (27)$$

$$\begin{cases} y = -4.229 - 0.037304x \\ z = 595.635 - 0.213728x \end{cases} \quad (28)$$

$$\begin{cases} y = -12.092 - 0.028561x \\ z = 596.189 - 0.214517x \end{cases} \quad (29)$$

For the plane lap workpiece model, Edge1 and Edge2 need to be sorted for subsequent weld extraction due to the drop between the workpiece planes. When shooting with a 3D camera, the z -axis is basically perpendicular to the workpiece plane. Therefore, when the features are the same, the z value of the weld edge of the lower layer is larger. Eq. 30 and Eq. 31 show the fitting equations of the lower weld edge Edge1 and upper weld edge Edge2, respectively.

$$\begin{cases} y = 2.855 - 0.022330x \\ z = 594.905 - 0.213805x \end{cases} \quad (30)$$

$$\begin{cases} y = -2.077 - 0.012751x \\ z = 590.145 - 0.215318x \end{cases} \quad (31)$$

Finally, the fitting effect of the weld edge lines is shown in Fig. 17.

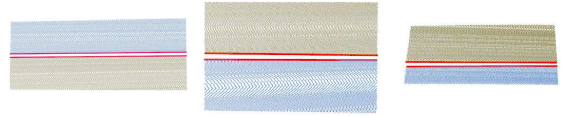


Fig. 17 Fitted weld edge lines

4.3 Solving weld equation

We set the fitting equations of Edge1 and Edge2 to be f_{E1} and f_{E2} , and the fitting equations of the three welds to be f_V , f_I and f_D . Analyze the geometric relationship between Edge1 and Edge2 of each workpiece and its weld, and solve the weld equation.

As shown in Fig. 18(a), due to the symmetry of the weld, the weld of the plane V-type butt workpiece model is obtained by shifting the midline of Edge1 and Edge2 downward by the groove depth d . The Eq. 32 can be obtained, where \vec{n}_V is the normal vector of the upper plane of the workpiece pointing to the lower plane.

$$f_V = \frac{f_{E1} + f_{E2}}{2} + d \times \vec{n}_V \quad (32)$$

The solution to \vec{n}_V is shown in Fig. 19. First, select three non-collinear points A , B , and C on the plane, use these three points to form any two vectors, and normalize the vector product of the two vectors to be the normal vector \vec{n}_1 of the

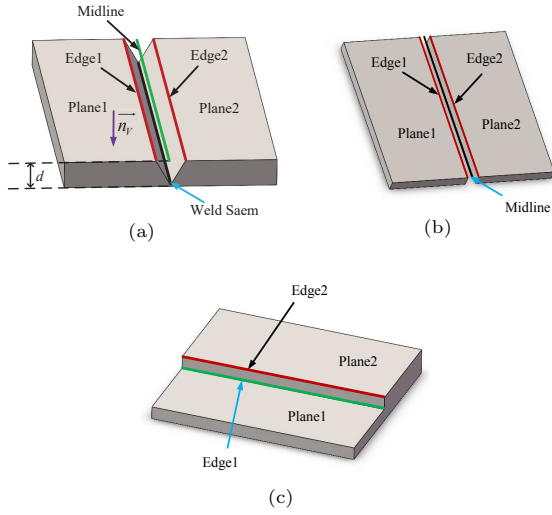


Fig. 18 Schematic diagram of plane welds extraction

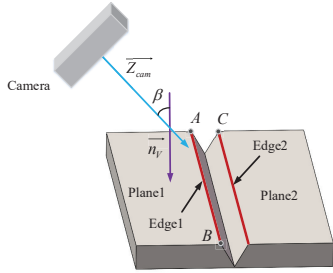


Fig. 19 Schematic diagram of plane normal vector solution

plane. Here, in order to reduce the amount of computation, we choose the endpoints of Edge1 and Edge2. Eq. 33 shows the solution of \vec{n}_1 .

$$\vec{n}_1 = \frac{\vec{AB} \times \vec{BC}}{\|\vec{AB} \times \vec{BC}\|} \quad (33)$$

Then, according to the shooting posture of the camera, the angle β between the positive direction of the z axis of the camera coordinate system and \vec{n}_1 is an acute angle. Therefore, take the inner product of \vec{n}_1 and the unit vector $\vec{Z}_{cam}(0, 0, 1)$ in the positive direction of the z -axis of the camera coordinate system, and adjust the direction of \vec{n}_1 according to the inner product to obtain \vec{n}_V . \vec{n}_V

can be solved by:

$$\vec{n}_V = \begin{cases} \vec{n}_1, & \vec{n}_1 \cdot \vec{Z}_{cam} \geq 0 \\ -\vec{n}_1, & \vec{n}_1 \cdot \vec{Z}_{cam} < 0 \end{cases} \quad (34)$$

After measurement, the groove depth d is $5mm$, yielding $\vec{n}_V = (0.127008, -0.0211309, 0.991677)$. It is known that f_{E1} and f_{E2} of the plane V-type butt workpiece weld have the form of Eq. 26 and Eq. 27. Substitute them into Eq. 32, and the equation of the weld can be obtained, as shown in Eq. 35.

$$\begin{cases} y = 1.8903 - 0.008513x \\ z = 776.9454 - 0.127546x \end{cases} \quad (35)$$

Finally, according to the definition domain, after the line is translated, after sampling the equation according to a certain step size, the obtained weld line is shown in Fig. 20(a), where the red points represent the weld.

As shown in Fig. 18(b), due to the symmetrical characteristics of the weld, the weld of the plane I-type butt workpiece model is the midline of Edge1 and Edge2. The available formula is Eq. 36.

$$f_I = \frac{f_{E1} + f_{E2}}{2} \quad (36)$$

f_{E1} and f_{E2} of the known plane I-type butt workpiece weld are Eq. 28 and Eq. 29. Substitute them into Eq. 36, and the equation of the weld can be obtained, as in Eq. 37. Finally, the weld is obtained as shown in Fig. 20(b).

$$\begin{cases} y = -8.196 - 0.037304x \\ z = 595.912 - 0.213728x \end{cases} \quad (37)$$

As shown in Fig. 18(c), the weld of the plane lap workpiece model is Edge1. It is known that the f_{E1} of the weld of the plane lap workpiece is Eq. 30. That is, the equation of the weld is Eq. 30. Finally, the weld is obtained as shown in Fig. 20(c).

$$f_D = f_{E1} \quad (38)$$

5 Experiments and results

The extracted welds are located in the camera coordinate system. In order to realize the welding

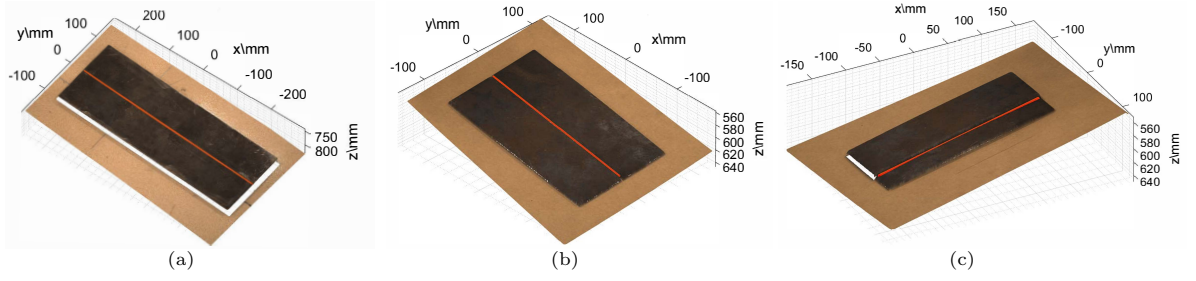


Fig. 20 Plane welds extraction results

trajectory planning, we first convert the welding seam feature points to the robot base coordinate system and then sample the feature points according to the robot's path control rules to form the robot's welding trajectory. Finally, a comparative experiment is designed, and the experimental results are analyzed to verify the rapidity, accuracy, and feasibility of the proposed method in this paper.

5.1 Welding trajectory planning

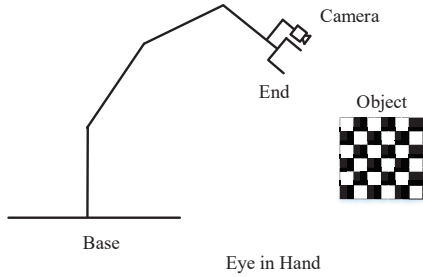


Fig. 21 Schematic diagram of hand-eye calibration[18]

Converting the weld feature points to the robot base coordinate system requires a high-precision hand-eye calibration. As shown in Fig. 21, in the process of hand-eye calibration, the positions of the robot's base and the calibration plate are fixed. And when the robot shoots the calibration board in different poses, the camera position relative to the robot's end is also unchanged. Therefore, there is a relationship in the calibration process, as shown in Eq. 39, where T represents the homogeneous transformation matrix[23].

$$\begin{aligned} & {}^{Base}T_{End2} {}^{End2}T_{Camera2} {}^{Camera2}T_{Object} \\ &= {}^{Base}T_{End1} {}^{End1}T_{Camera1} {}^{Camera1}T_{Object} \quad (39) \end{aligned}$$

After shifting the terms in Eq. 39, we can get:

$$\begin{aligned} & {}^{Base}T_{End1}^{-1} {}^{Base}T_{End2} {}^{End2}T_{Camera2} \\ &= {}^{End1}T_{Camera1} {}^{Camera1}T_{Object} {}^{Camera2}T_{Object}^{-1} \quad (40) \end{aligned}$$

Because ${}^{End2}T_{Camera2} = {}^{End1}T_{Camera1}$, the problem is transformed into a solution problem of $AX = XB$. By taking multiple shots in different robot poses, ${}^{End}T_{Camera}$ can be obtained at the end.

$${}^{End}T_{Camera} = \begin{bmatrix} 0.9943 & 0.0364 & -0.1003 & 76.0178 \\ -0.353 & 0.9993 & 0.0121 & -84.3385 \\ 0.1007 & -0.0085 & 0.9949 & 100.3920 \\ 0 & 0 & 0 & 1.0 \end{bmatrix} \quad (41)$$

We need to transform the points in the camera coordinate system into the base coordinate system through the transformation matrix ${}^{Base}T_{Camera}$. The formula is shown in Eq. 42, where p denotes any point in space.

$$\begin{aligned} & {}^{Base}p = {}^{Base}T_{Camera} {}^{Camera}p \\ &= {}^{Base}T_{End} {}^{End}T_{Camera} {}^{Camera}p \quad (42) \end{aligned}$$

In this experiment, the robot poses when shooting the plane V-type butt-joint workpiece model, the plane I-type butt-joint workpiece model, and the plane lap joint workpiece model are: $(-613.50, -284.81, 296.28, 178.28, 1.04, 107.12)$, $(-516.72, -231.54, 186.02, 176.89, 6.33, 105.70)$ and $(-516.72, -231.54, 186.02, -176.89, 6.33, 105.70)$, respectively. The format of the pose data is (x, y, z, rx, ry, rz) , the first three variables are coordinate values in mm , and the last three are RPY angle values in degrees. Converting the

robot pose data into a homogeneous coordinate matrix is ${}^{Base}T_{End}$.

Finally, bring the fitted weld points into Eq. 42 to get the weld in the robot Base coordinate system, as shown in Fig. 22.

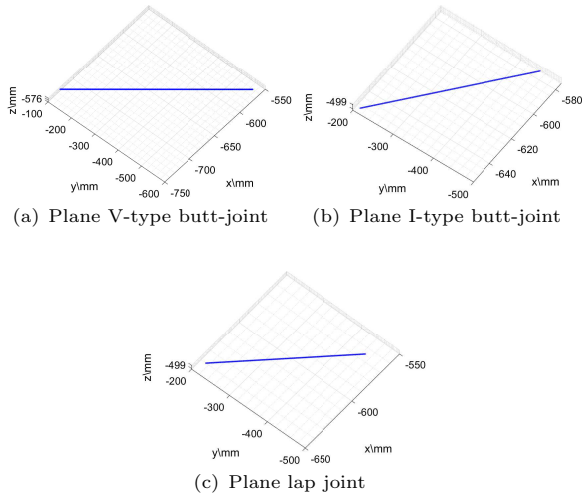


Fig. 22 Weld seams in the robot base coordinate system

5.2 Experimental result analysis

In order to verify the accuracy of the welding track, we take the manual teaching welding method as the benchmark and compare the taught track with the welding track obtained in this experiment for error analysis.

First, we manually teach points for three kinds of welds and take 12 points for each weld. As shown in Fig. 23, the black points are the teaching points, and the blue lines are the welding trajectories obtained by the experiment. Then, calculate the minimum distance from each manual teaching point to the obtained welding trajectory straight line, which represents the error between the manual welding method and the method in this paper. Finally, the error analysis is obtained in Fig. 24.

As shown in Fig. 24, for the welding trajectory planning of the plane weld, the errors of the proposed method are stable within 1mm. This accuracy fully meets the error requirements of industrial welding scenarios. Therefore, this paper's welding trajectory planning method can completely replace the manual teaching method.

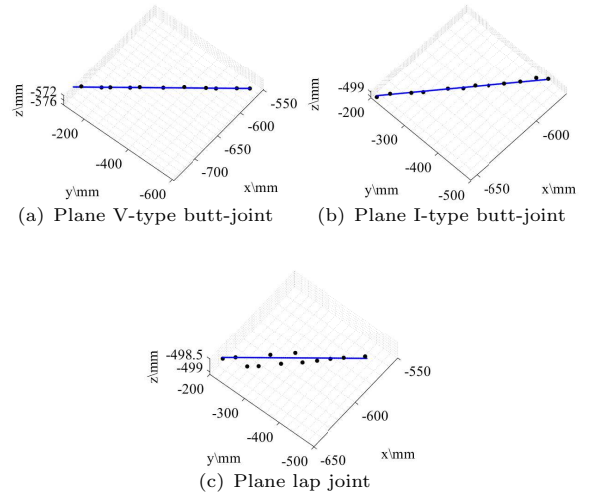


Fig. 23 Comparison diagram of manually taught trajectory and obtained trajectory

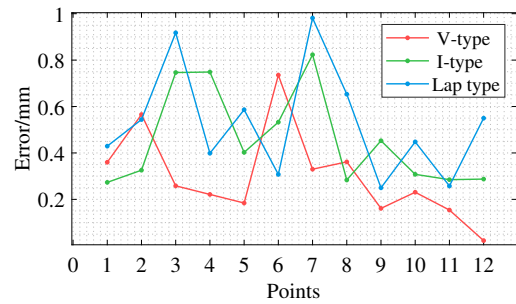


Fig. 24 Error Analysis Chart

At the end of the experiment, according to the programming rules of the robot controller, we reasonably sample the fitting point cloud of the welding seam to obtain the robot welding trajectory points. After reasonably planning the robot's end pose, the obtained welding trajectory points are sent to the robot controller. The robot can drive the welding torch to perform the welding task accurately, which further verifies the feasibility and accuracy of the method.

5.3 Algorithm efficiency analysis

In industrial sites, efficiency improvement is one of the main motivations for automated equipment to replace manual labor. The algorithm design of this experiment was initially deduced using Matlab and finally implemented using C++.

Due to the large point cloud data, this experiment uses multi-threaded programming, which improves the algorithm's efficiency. Through many experiments, we finally get the average running time of the algorithm, as shown in Table 2.

Table 2 Algorithm running time

Step	Running time(ms)
The camera gets point cloud	800
Welding path planning	3508
The whole process	4308

It can be seen from Table 2 that the time for this algorithm to process the point cloud of a plane weld is 4.308s. Therefore, the algorithm meets the efficiency requirements in industrial welding scenarios and has rapidity.

6 Conclusion

Facing industrial requirements, this paper proposes a novel 3D vision-based plane weld trajectory planning method. This method finally realizes the automatic robot welding of three types of plane welds without teaching and programming. The advantages of this method are as follows:

1. This method liberates labor, improves welding efficiency, and solves the problems of poor manual welding precision and consistency.
2. The method realizes the automatic trajectory planning of the plane welding workpiece, avoids the complicated programming work of the welding robot, and improves the automation degree of the robot welding.

Declarations

Ethical Approval

Not applicable.

Consent to Participate

Not applicable.

Consent to Publish

Not applicable.

Authors Contributions

Yuankai Zhang was a major contributor in writing the manuscript. All authors read and approved the final manuscript.

Funding

This work was supported by the National Natural Science Foundation of China (No. U20A20201), Shandong Provincial Key Research and Development Program (2022CXGC010101), Taishan Industry Leading Talent Project, Shandong Provincial Natural Science Foundation (No. ZR2021QF024), and Shandong Provincial Postdoctoral Innovation Program (No. 202102009).

Competing Interests

The authors declare that they have no conflict of interest.

Availability of data and materials

Not applicable.

References

- [1] Wang, X., Zhou, X., Xia, Z., Gu, X.: A survey of welding robot intelligent path optimization. *Journal of Manufacturing Processes* **63**, 14–23 (2021)
- [2] Maiolino, P., Woolley, R., Branson, D., Benardos, P., Popov, A., Ratchev, S.: Flexible robot sealant dispensing cell using RGB-D sensor and off-line programming. *Robotics and Computer-Integrated Manufacturing* **48**, 188–195 (2017)
- [3] Hou, Z., Xu, Y., Xiao, R., Chen, S.: A teaching-free welding method based on laser visual sensing system in robotic GMAW. *The International Journal of Advanced Manufacturing Technology* **109**(5), 1755–1774 (2020)
- [4] Wu, Z.-l., Sun, C.-k.: Modeling and parameters analysis of vision measuring sensor. In: 2010 International Conference on Computer, Mechatronics, Control and Electronic Engineering, vol. 2, pp. 84–87 (2010). IEEE
- [5] Geng, J.: DLP-based structured light 3D imaging technologies and applications. In:

- Emerging Digital Micromirror Device Based Systems and Applications III, vol. 7932, pp. 95–109 (2011). SPIE
- [6] Li, Z., Cui, J., Wu, J., Tan, J.: Structural parameters analysis and optimization of line-structured light measuring system. In: 2016 23rd International Conference on Mechatronics and Machine Vision in Practice (M2VIP), pp. 1–6 (2016). IEEE
- [7] Xu, Y., Yu, H., Zhong, J., Lin, T., Chen, S.: Real-time seam tracking control technology during welding robot GTAW process based on passive vision sensor. *Journal of Materials Processing Technology* **212**(8), 1654–1662 (2012)
- [8] Kiddee, P., Fang, Z., Tan, M.: An automated weld seam tracking system for thick plate using cross mark structured light. *The International Journal of Advanced Manufacturing Technology* **87**(9-12), 3589–3603 (2016)
- [9] Liang, B., Xu, X., Gong, S., Wang, Q., Wang, X.: Dual-beam laser welding and seam tracking control technology for 3D T-beam. *Transactions of the China Welding Institution* **37**(2), 47–50 (2016)
- [10] Shao, W.J., Huang, Y., Zhang, Y.: A novel weld seam detection method for space weld seam of narrow butt joint in laser welding. *Optics & Laser Technology* **99**, 39–51 (2018)
- [11] Gao, Y., Zhong, P., Tang, X., Hu, H., Xu, P.: Feature Extraction of Laser Welding Pool Image and Application in Welding Quality Identification. *IEEE Access* **9**, 120193–120202 (2021)
- [12] Jing, L., Fengshui, J., En, L.: RGB-D sensor-based Auto Path Generation Method for Arc Welding Robot. In: Proceedings of the 28th Chinese Control and Decision Conference (2016 Ccdc), pp. 4390–4395. IEEE, New York (2016)
- [13] Ahmed, S.M., Tan, Y.Z., Chew, C.M., Mamun, A.A., Wong, F.S.: Edge and Corner Detection for Unorganized 3D Point Clouds with Application to Robotic Welding. In: 2018 IEEE/RSJ International Conference on Intelligent Robots and Systems (IROS), pp. 7350–7355. IEEE, Madrid (2018)
- [14] Peng, R., Navarro-Alarcon, D., Wu, V., Yang, W.: A point cloud-based method for automatic groove detection and trajectory generation of robotic arc welding tasks. In: 2020 17th International Conference on Ubiquitous Robots (UR), pp. 380–386 (2020). IEEE
- [15] Gao, Y., Ping, C., Wang, L., Wang, B.: A Simplification Method for Point Cloud of T-Profile Steel Plate for Shipbuilding. *Algorithms* **14**(7), 202 (2021)
- [16] Patil, V., Patil, I., Kalaiichelvi, V., Karthikeyan, R.: Extraction of Weld Seam in 3D Point Clouds for Real Time Welding Using 5 DOF Robotic Arm. In: 2019 5th International Conference on Control, Automation and Robotics (ICCAR), pp. 727–733. IEEE, Beijing, China (2019)
- [17] Gao, J., Li, F., Zhang, C., He, W., He, J., Chen, X.: A Method of D-Type Weld Seam Extraction Based on Point Clouds. *IEEE Access* **9**, 65401–65410 (2021)
- [18] Geng, Y., Zhang, Y., Tian, X., Shi, X., Wang, X., Cui, Y.: A method of welding path planning of steel mesh based on point cloud for welding robot. *The International Journal of Advanced Manufacturing Technology* **116**(9), 2943–2957 (2021)
- [19] Geng, Y., Zhang, Y., Tian, X., Shi, X., Wang, X., Cui, Y.: A novel welding path planning method based on point cloud for robotic welding of impeller blades. *The International Journal of Advanced Manufacturing Technology*, 1–14 (2022)
- [20] Yang, L., Liu, Y., Peng, J., Liang, Z.: A novel system for off-line 3D seam extraction and path planning based on point cloud segmentation for arc welding robot. *Robotics and Computer-Integrated Manufacturing* **64**, 101929 (2020)
- [21] Wang, Z.: Review of real-time three-dimensional shape measurement techniques.

Measurement **156**, 107624 (2020)

- [22] Fischler, M.A., Bolles, R.C.: Random sample consensus: a paradigm for model fitting with applications to image analysis and automated cartography. *Communications of the ACM* **24**(6), 381–395 (1981)
- [23] Li, M., Du, Z., Ma, X., Dong, W., Gao, Y.: A robot hand-eye calibration method of line laser sensor based on 3D reconstruction. *Robotics and Computer-Integrated Manufacturing* **71**, 102136 (2021)